Curvature Integrability of Subdivision Surfaces

Ulrich Reif [a] Peter Schröder [b]

[a] *Technische Universität Darmstadt*
E-mail: reif@mathematik.tu-darmstadt.de
[b] *Caltech*
E-mail: ps@cs.caltech.edu

Received 2 February 2000; revised 9 September 2000; accepted 15 November 2000

We examine the smoothness properties of the principal curvatures of subdivision surfaces near irregular points. In particular we give an estimate of their L_p class based on the eigenstructure of the subdivision matrix. As a result we can show that the popular Loop and Catmull-Clark schemes (among many others) have square integrable principal curvatures enabling their use as shape functions in FEM treatments of the thin shell equations.

Keywords: Subdivision, smoothness, function spaces, approximation, thin shell equations

AMS Subject classification: 65D17, Computer Aided Design (modeling of curves and surfaces); 65N30, Finite Elements, Rayleigh-Ritz and Galerkin methods

1. Introduction

Subdivision surfaces are a popular modeling primitive in computer graphics and computer assisted geometric design. They offer many advantages in applications, chief among them their ability to model smooth surfaces of arbitrary topology. Figure 1 shows examples of surfaces based on the scheme of Loop [13] (left) and Catmull-Clark [3] (right).

Historically subdivision schemes were developed as generalizations of uniform B-spline (midpoint) knot insertion algorithms [5] to settings with topologically irregular control meshes, i.e., those with vertices whose valence is other than four. Doo and Sabin [6] generalized bi-quadratic splines, while Catmull and Clark [3] generalized bi-cubic splines in this way. Similarly, Loop [13] generalized quartic box splines (in this case irregular vertices are those with valence other than six) and Habib and Warren [8] as well as Peters and Reif [14] generalized the quadratic 4-direction spline. The idea of subdivision was also studied independent of the spline setting. For example, Dyn et al. [7] (and later Zorin et al. [25]) described an interpolating scheme based on triangles, while Leber [12] and Kobbelt [11] developed interpolating schemes based on quadrilaterals.

In all these settings smooth surfaces are created through a limit process of recursive refinement of a given initial polyhedron. For example, in the Loop scheme an initial 2-

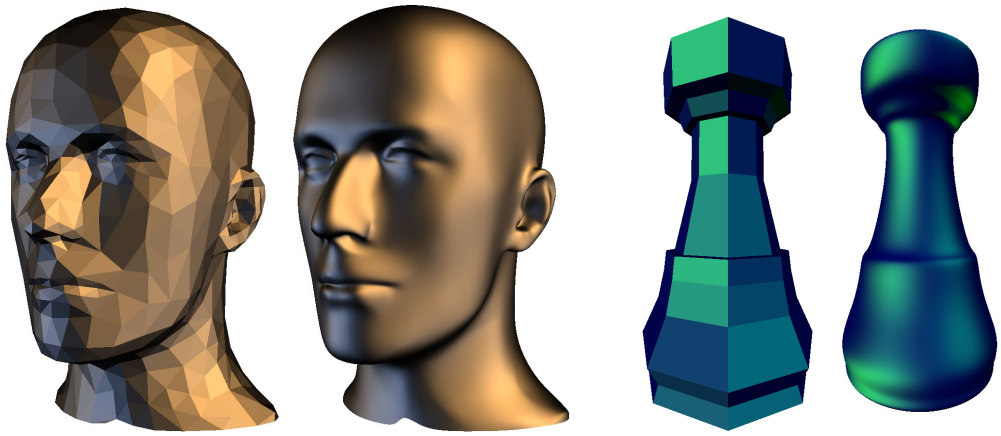

Figure 1. Examples of smooth surfaces built with the scheme of Loop (left) and with the Catmull-Clark scheme (right). In both cases the control mesh is shown on the left, while the right hand side shows the resulting surface.

manifold (possibly with boundary) triangle mesh is refined by splitting each triangle into four with new point positions defined as simple local averages of old point positions of the coarser mesh (see Figure 2 which shows the split rule and associated weighting stencils). The weights used in the averaging operator depend only on the valence of the vertices partaking in it. Choosing the weights carefully it can then be shown that the limit surface is smooth in the sense that it possesses a regular parameterization everywhere. The analysis involves the eigenstructure of the subdivision operator together with an analysis of the characteristic map [17].

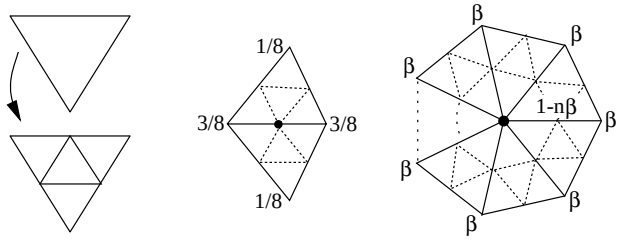

Figure 2. The scheme of Loop splits each triangle of the control mesh into four. Point positions for new vertices are computed as averages of four neighbors (middle), while point positions for old vertices are recomputed as averages of their immediate neighbors (right) using a weight β depending on the valence of the center vertex.

Because the resulting surfaces are a linear combination of smooth basis functions, a natural question that arises is whether these basis functions can serve as the shape functions in a FEM simulation of the mechanical properties of the described surface. From a practical point of view a positive answer to this question opens up the possibility of unifying surface representations used in a geometric modeling application with

those used by FEM solvers. Of particular interest in this context is the modeling of thin shell equations describing the behavior of flexible structures such as those made of sheet metal, for example, in the automobile or aerospace industries.

Applying Kirchhoff-Love theories [21] to the modeling of thin shell equations requires the shape functions to have square integrable curvatures. In this paper we examine the question whether the principal curvatures of subdivision surfaces near irregular points are square integrable. More precisely we give an estimate of the L_p space containing the principal curvatures.

1.1. Overview

We begin with a brief overview of the two most commonly used subdivision schemes due to Loop and Catmull-Clark. This serves to establish the general setup before we proceed to a brief review of the analysis of general subdivision schemes. Our main result uses this foundation to give an estimate of the L_p space containing the principal curvatures of subdivision surfaces. We conclude with a brief section presenting some numerical examples.

2. Setup

In the most general terms, subdivision defines smooth surfaces of arbitrary topology through a limiting process of repeated refinement applied to an initial control polyhedron. A number of such schemes have been studied in the literature (for an overview see [24]). Here we are particularly interested in the schemes of Loop [13] and Catmull-Clark [3], which are generalizations of spline patch methods based on triangles and quadrilaterals respectively.

The Loop scheme begins with a control polyhedron in $\mathbb{R}^3$ consisting only of triangles, which form a topological 2-manifold possibly with boundary. A refinement step consists of quadrisecting each triangle and computing new point positions for newly introduced vertices as well as those vertices inherited from the coarser control mesh. The associated stencils are given in Figure 2. There is some freedom when choosing the parameter β. Loop's original choice [13] was

$$\beta = \frac{1}{8n}\left(5 - \frac{(3 + 2\cos(\frac{2\pi}{n}))^2}{8}\right),$$

while Warren [22] suggested

$$\beta = \begin{cases} \frac{3}{8n} & n > 3 \\ \frac{3}{16} & n = 3 \end{cases}.$$

The surfaces resulting from these two choices are visually indistinguishable. Warren's choice has the advantage that the expressions for eigenvalues and eigenvectors of the subdivision matrix are significantly simplified. For some of the numerical experiments later on we will use Warren's choice.

An important aspect of subdivision is the fact that all newly inserted vertices are regular, i.e., their valence is six. Consequently the refined control polyhedra consist of ever larger sections of mesh which are entirely regular with only isolated vertices whose valence is other than six (irregular vertices). In the regular setting when all vertices have valence six the subdivision rules reproduce the refinement rules for quartic box splines. Consequently the limit surface consists of quartic box spline patches almost everywhere. The irregular vertices are at the center of irregular patches which can be thought of as consisting of an infinite geometric sequence of rings of regular patches (see Figure 3).

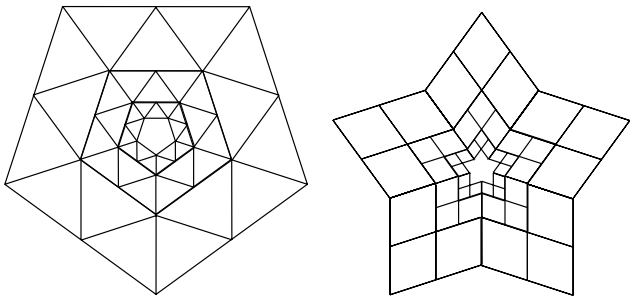

Figure 3. Since new vertices inserted during subdivision always carry the canonical valence (4 for quad schemes, 6 for triangle schemes) we can think of the vicinity of an irregular point as being at the center of an infinite sequence of ever smaller rings of regular patches. Here the case $k = 5$ is illustrated for the schemes of Loop (left) and Catmull-Clark (right) for a few such rings converging to the center.

Because of these observations the analytic properties of the limit surface are given by the properties of quartic box splines, except at the irregular vertices. The behavior of the surface at the irregular vertices can be determined by analyzing the local subdivision operator around these vertices, its eigenvalues and (generalized) eigenvectors, and the characteristic map [17]. In the case of the Loop scheme the surface is globally C^2 except at the irregular vertices where it is only C^1 [20].

For completeness we mention that one can develop appropriately modified stencils for boundaries and surface features such as creases and corners [10,20,2].

The scheme of Catmull and Clark generalizes bi-cubic splines to arbitrary topology control meshes. In this case the initial polyhedron consists entirely of quadrilaterals. Subdivision proceeds as before by quadrisection, i.e., every face is replaced by four faces (see Figure 4, left). This time three different stencils are required for the computation of new point positions: vertex, edge, and face stencils (see Figure 4, middle and right). All new vertices have valence four while only the original control polyhedron vertices may have valence other than four. The parameters for the irregular vertex stencil (Figure 4, right) may be chosen as $\beta = 3/(2n^2)$, $\gamma = 1/(4n^2)$.

In the regular setting, i.e., when vertices have valence four the Catmull-Clark scheme reproduces the (midpoint) knot insertion rules for uniform bi-cubic splines. Consequently the surface is globally C^2 as before with the exception of irregular vertices where the surface is C^1 [15]. Once again a number of modifications near boundaries

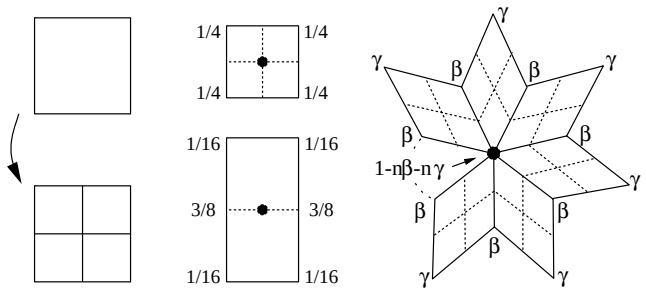

Figure 4. In the case of Catmull-Clark subdivision there are three types of rules for point positions. Those associated with faces (middle top), edges (middle bottom), and vertices (right) in the coarser mesh.

and creases which rely on simple modifications of the subdivision stencils have been demonstrated (see for example the treatment in [2]).

3. Analysis

All subdivision schemes are characterized by producing meshes which are regular (valence six for triangles, four for quadrilaterals) over increasingly larger regions. Only a finite number of irregular vertices remain which are increasingly more isolated. Together with the local support of the subdivision rules this implies that the analysis of the limit surface reduces to the regular case almost everywhere. Smoothness analysis in the regular parts of the mesh relies on Fourier techniques. The situation is different around irregular vertices where the lack of translation invariance prohibits the use of Fourier tools. Instead the smoothness analysis relies on spectral analysis of the local subdivision operator and properties of the induced *characteristic map*.

In this section we analyze the integrability of the principal curvatures of symmetric subdivision schemes. In the first subsection, we introduce notation. Then, the asymptotic behavior of the first and second fundamental form is studied, and finally, we present results on the asymptotic behavior of the principal curvatures and their membership in L_p-spaces.

3.1. Subdivision Surfaces Built from Splines

The setup described here applies to arbitrary linear stationary subdivision schemes, and in particular to all non-variational methods currently in use, for example, the algorithms of Catmull-Clark, Doo-Sabin, and Loop. In order to investigate analytic properties of subdivision surfaces, we regard them as a union of parameterized surface patches rather than as the limit of finer and finer control meshes.

More precisely, near an irregular vertex of valence n, we parametrize a subdivision surface $\mathbf{s}$ by a union of *spline rings* $\mathbf{s}_m$,

$$\mathbf{s} := \bigcup_{m\in\mathbb{N}} \mathbf{s}_m \,.$$

In turn, each surface ring

$$\mathbf{s}_m := \bigcup_{j\in\mathbb{Z}_n} \mathbf{s}_{m,j}\,, \quad m \in \mathbb{N}\,,$$

is a union of n *patches*

$$\mathbf{s}_{m,j} : \mathbb{R}^2 \supset \omega \to \mathbb{R}^3\,, \quad j \in \mathbb{Z}_n\,,$$

where $\mathbb{Z}_n$ denotes the set of integers modulo n. A natural choice of the domain ω depends on whether the considered scheme is based on triangular or quadrilateral meshes,

$$\omega := \begin{cases} \{(u,v) \in \mathbb{R}^2_{\geq 0} : 1 \leq u+v \leq 2\} & \text{for triangular schemes} \\ \{(u,v) \in \mathbb{R}^2_{\geq 0} : 1 \leq \max(u,v) \leq 2\} & \text{for quadrilateral schemes,} \end{cases}$$

(see Figure 5). For the analysis, the specific type of ω is completely irrelevant; subsequent Figures exemplarily refer to the quadrilateral case. The domain $\Omega := \omega \times \mathbb{Z}_n$ of a spline ring consists of n copies of ω. A topology on Ω is defined by identifying pairs of edges according to Figure 3. A comprehensive exposition of the formal structure of spline surfaces is given in [18].

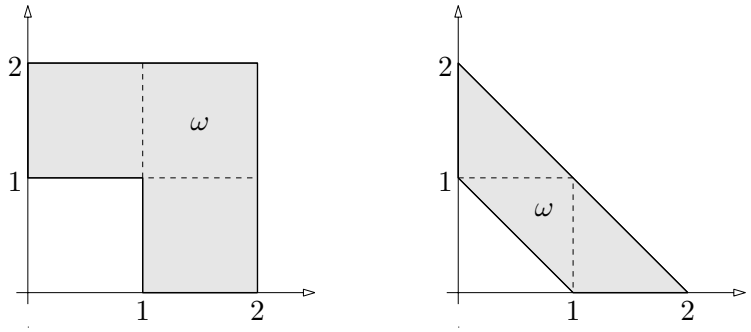

Figure 5. Domain ω for schemes bases on quadrilateral meshes (left) and triangular meshes (right).

In order to be able to analyze linear stationary subdivision schemes with finite mask size, we assume the following: All spline rings lie in a common finite-dimensional space spanned by continuous, piecewise twice differentiable functions $\varphi_0, \ldots, \varphi_Q : \Omega \to \mathbb{R}$ forming a partition of unity,

$$\sum_{q=0}^{Q} \varphi_j = 1\,.$$

Each spline ring can be expressed as a linear combination of these functions with coefficients $\mathbf{B}_m^0, \ldots, \mathbf{B}_m^Q$ in $\mathbb{R}^3$. Collecting the functions in a row vector $\boldsymbol{\varphi} := [\varphi_0, \ldots, \varphi_Q]$ and the coefficients in a $(Q+1) \times 3$-matrix $\mathbf{B}_m := [\mathbf{B}_m^1; \ldots; \mathbf{B}_m^Q]$, we write

$$\mathbf{s}_m = \sum_{q=0}^{Q} \varphi_q \mathbf{B}_m^q = \boldsymbol{\varphi} \mathbf{B}_m \,. \tag{1}$$

For *linear stationary schemes*, the sequence of coefficient matrices is generated recursively by application of a square matrix S starting from the *initial data* $\mathbf{B}_0$,

$$\mathbf{B}_m = S\mathbf{B}_{m-1} \,, \quad \mathbf{B}_m = S^m \mathbf{B}_0 \,, \quad m \in \mathbb{N} \,. \tag{2}$$

Here, stationarity refers to the fact that the same matrix S is applied at each step of the recursion. Further, we assume that all rows of S sum up to 1 reflecting the fact that all subdivision schemes considered here are affine invariant,

$$S\mathbf{e} = \mathbf{e} \,, \quad \mathbf{e} = [1; \ldots; 1] \,. \tag{3}$$

3.2. The Spectrum of the Subdivision Matrix

The spectrum of the matrix S plays an important role in the analysis of subdivision algorithms. Since the functions in $\boldsymbol{\varphi}$ are not necessarily linearly independent, there might exist whole classes of matrices which are equivalent in the sense that they generate equal sequences of spline rings. In particular, there might exist eigenspaces of S corresponding to arbitrary eigenvalues which are anihilated by $\boldsymbol{\varphi}$ and hence do not affect the scheme. In order to be able to relate smoothness properties of the generated surfaces to the spectrum of S, we chose from a class of equivalent matrices a generic representative. Let

$$W_{\boldsymbol{\varphi}} := \{\mathbf{v} \in \mathbb{R}^{Q+1} : \boldsymbol{\varphi}\mathbf{v} = 0\}$$

denote the kernel of $\boldsymbol{\varphi}$, then we call S a *subdivision matrix*, if it satisfies

$$V_{\boldsymbol{\varphi}} := \bigcap_{n \in \mathbb{N}_0} S^m W_{\boldsymbol{\varphi}} \subset \ker S. \tag{4}$$

In other words, we require that all invariant subspaces which are anihilated by $\boldsymbol{\varphi}$ correspond to vectors of control points which lie in the kernel of S. Le Π be a projector onto the subspace $V_{\boldsymbol{\varphi}}$ with $\Pi\mathbf{e} = 0$, then $S' := (\mathrm{Id} - \Pi)S$ is a subdivision matrix which is equivalent to S, see [18] for a simple proof. Hence, we can assume (4) without loss of generality.

Under mild non-degeneracy assumptions, one can show that there exist exactly five classes of subdivision matrices, characterized by the structure of their Jordan normal form, which are capable of generating tangent plane continuous surfaces [18,23]. To keep technical requirements to a minimum we limit ourselves to the discussion of symmetric schemes. These are of most interest in applications.

We denote the sequence of all (possibly complex) eigenvectors of S by $\mathbf{v}_0, \ldots, \mathbf{v}_P$ and the corresponding eigenvalues by $\lambda_0, \ldots, \lambda_P$, i.e.,

$$S\mathbf{v}_j = \lambda_j \mathbf{v}_j\,, \quad j = 0, \ldots, P\,.$$

The algebraic multiplicities of the eigenvalues are $L_0 + 1, \ldots, L_P + 1$, hence $L_0 + \cdots + L_P = Q - P$. To the eigenvalue λ_j corresponds a $(L_j + 1)$-dimensional S-invariant subspace, spanned by a chain of generalized eigenvectors $\mathbf{w}_j^0, \ldots, \mathbf{w}_j^{\nu_j}$ starting from the eigenvector $\mathbf{w}_j^0 = \mathbf{v}_j$,

$$\begin{aligned} S\mathbf{w}_j^0 &= \lambda_j \mathbf{w}_j^0 \\ S\mathbf{w}_j^k &= \lambda_j \mathbf{w}_j^k + \mathbf{w}_j^{k-1}\,, \quad k = 1, \ldots, L_j\,. \end{aligned}$$

Powers of S applied to generalized eigenvectors yield

$$S^m \mathbf{w}_j^k = \tbinom{m}{k} \lambda_j^{m-k} \mathbf{v}_j (1 + O(1/m)) = O(m^k \lambda_j^m)\,. \tag{5}$$

Here and subsequently, the Landau symbol refers to $m \to \infty$. For vectors and matrices, it is understood component-wise, and for functions in a uniform sense.

The sequence $S^m \mathbf{w}_j^k$ obtained for $k = L_j$ dominates all others with lower index. According to the maximal growth of sequences in the corresponding invariant subspaces, we order eigenvalues primarily by modulus, and secondarily by algebraic multiplicity,

$$\begin{gathered} |\lambda_0| \geq |\lambda_1| \geq \cdots \geq |\lambda_Q| \\ L_j \geq L_{j+1} \quad \text{if} \quad |\lambda_j| = |\lambda_{j+1}|\,. \end{gathered}$$

By (3), 1 is an eigenvalue of S to the eigenvector $\mathbf{e} = [1; \ldots; 1]$. The moduli of all other eigenvalues of S have to be strictly less than 1 in order to guarantee that the sequence of spline rings converges to a unique limit. More precisely, we require

$$1 = \lambda_0 > |\lambda_1|\,, \quad L_0 = 0\,,$$

hence $\mathbf{v}_0 = \mathbf{e}$. Symmetric tangent plane continuous subdivision schemes are known to have a double real *subdominant eigenvalue* [15]. This means that there exists a pair

$$(\lambda_1, L_1) = (\lambda_2, L_2)$$

of real eigenvalues with equal multiplicity, and for the third eigenvalue we have either

$$|\lambda_3| < |\lambda_1|$$

or

$$|\lambda_3| = |\lambda_1|\,, \quad L_3 < L\,.$$

For convenience, we introduce the notation

$$\lambda := \lambda_1 = \lambda_2\,, \quad \mu := |\lambda_3|\,, \quad L := L_1 = L_2\,, \quad M := L_3\,. \tag{6}$$

For most subdivision algorithms of practical relevance, the subdominant eigenvalue λ is double and strictly greater in modulus than the third one, i.e., $L = 0$ and $\mu < \lambda$. In

this case, we speak of a *strongly subdominant eigenvalue* (SSE). Conversely, a *weakly subdominant eigenvalue* (WSE) refers to $L > 0$, regardless of whether $\mu < \lambda$ or $\mu = \lambda$ and $M < L$. Although there exist algorithms with such an eigenstructure [14], empirical evidence shows that they generate surfaces of lower quality. The results presented here suggest a theoretical explanation for this observation: Weakly subdominant eigenvalues yield just square integrability of the principal curvatures, while strongly subdominant eigenvalues yield L_p-integrability for exponents $p < p^*$, where the bound p^* is always greater than 2 and monotone increasing with the ratio $\ln|\lambda|/\ln\mu$. Since p^* can be regarded as a measure for the rate of divergence of the principal curvatures, the relation between this and the visual quality of the generated surfaces becomes apparent.

3.3. The Characteristic Map

Combining Eqs. (1) and (2), we find

$$\mathbf{s}_m = \boldsymbol{\varphi} S^m \mathbf{B}_0\,, \quad m \in \mathbb{N}$$

for the sequence of spline rings. In order to apply our previous results, we write the initial data $\mathbf{B}_0$ as a linear combination of generalized eigenvectors,

$$\mathbf{B}_0 = \sum_{j=0}^{P} \sum_{k=0}^{L_j} \mathbf{w}_j^k \mathbf{b}_j^k \quad \mathbf{b}_j^k \in \mathbb{R}^3\,.$$

Letting $\mathbf{b}_1 := \mathbf{b}_1^{L_1}$ and $\mathbf{b}_2 := \mathbf{b}_2^{L_2}$, we obtain using $\boldsymbol{\varphi}\mathbf{v}_0 = 1$ and (5)

$$\mathbf{s}_m = \mathbf{b}_0^0 + \begin{cases} \lambda^m \boldsymbol{\varphi}(\mathbf{v}_1\mathbf{b}_1 + \mathbf{v}_2\mathbf{b}_2) + O\big(m^M \mu^m\big) & \text{for an SSE} \\ \binom{m}{L}\lambda^m \boldsymbol{\varphi}(\mathbf{v}_1\mathbf{b}_1 + \mathbf{v}_2\mathbf{b}_2) + O\big(m^{L-1}\lambda^m\big) & \text{for a WSE}\,. \end{cases}$$

In the limit, the scaled and translated spline rings

$$\tbinom{m}{L}^{-1}\lambda^{-m}(\mathbf{s}_m - \mathbf{b}_0^0) = \boldsymbol{\varphi}[\mathbf{v}_1, \mathbf{v}_2] \begin{bmatrix} \mathbf{b}_1 \\ \mathbf{b}_2 \end{bmatrix} + O(1/m)$$

tend to an affine image of the map

$$\Psi = \boldsymbol{\varphi}[\mathbf{v}_1, \mathbf{v}_2]$$

which is independent of the initial data and of major significance for the analysis. Therefore, it is called the *characteristic map* of the subdivision scheme. We note that the characteristic map is a non-zero *planar spline ring*, i.e., $\Psi : \Omega \to \mathbb{R}^2$. According to [17], a subdivision algorithm generates C^1-regular limit surfaces for almost all initial data $\mathbf{B}_0$ if the characteristic map is injective and regular in the sense that its Jacobian

$$J := \det D\Psi = \partial_u \boldsymbol{\varphi}\mathbf{v}_1\, \partial_v \boldsymbol{\varphi}\mathbf{v}_2 - \partial_u \boldsymbol{\varphi}\mathbf{v}_2\, \partial_v \boldsymbol{\varphi}\mathbf{v}_1$$

has no zeros. In contrast, C^1-regularity is impossible if J changes sign. Therefore, we shall assume regularity and injectivity of the characteristic map in the following.

3.4. Asymptotic Behavior of Fundamental Forms

In what follows, we assume that the limit surfaces generated by the subdivision algorithm are tangent plane continuous for almost all initial data and that the basis functions $\boldsymbol{\varphi}$ are piecewise C^2. In particular, C^1-variants of Doo-Sabin, Catmull-Clark, and the Loop scheme live up to this requirement, while the butterfly scheme is excluded by not being C^2.

In order to prepare our analysis of curvature properties of subdivision surfaces, we discuss the asymptotic behavior of the first and second fundamental form near an irregular point. Throughout, representations with respect to the standard basis $\{\partial_u \mathbf{s}_m, \partial_v \mathbf{s}_m\}$ are used.

The first fundamental form of the m-th spline ring $\mathbf{s}_m$ is

$$I_m = \begin{bmatrix} \langle \partial_u \mathbf{s}_m, \partial_u \mathbf{s}_m \rangle & \langle \partial_u \mathbf{s}_m, \partial_v \mathbf{s}_m \rangle \\ \langle \partial_u \mathbf{s}_m, \partial_v \mathbf{s}_m \rangle & \langle \partial_v \mathbf{s}_m, \partial_v \mathbf{s}_m \rangle \end{bmatrix} = O\big(m^{2L}\lambda^{2m}\big)\,.$$

A short computation shows that the determinant of I_m is related to the Jacobian of the characteristic map by

$$\det I_m = J^2 \tbinom{m}{L}^4 \lambda^{4m}\big(1 + O(1/m)\big)\,.$$

Since J is continuous and, by assumption, non-zero on the compact domain Ω, its reciprocal is bounded, and we find

$$\det I_m^{-1} = J^{-2} \tbinom{m}{L}^{-4} \lambda^{-4m}\big(1 + O(1/m)\big) \;= O\big(m^{-4L}\lambda^{-4m}\big)\,.$$

This implies for the inverse of the first fundamental form

$$I_m^{-1} = O\big(m^{-2L}\lambda^{-2m}\big)\,. \tag{7}$$

In order to compute the second fundamental form we consider the normal vector

$$\mathbf{n}_m = \frac{\partial_u \mathbf{s}_m \times \partial_v \mathbf{s}_m}{\|\partial_u \mathbf{s}_m \times \partial_v \mathbf{s}_m\|} = \sqrt{\det I_m^{-1}}\,(\partial_u \mathbf{s}_m \times \partial_v \mathbf{s}_m)\,.$$

By our previous results, this expression is well defined for m sufficiently large. The asymptotic behavior depends on whether λ is strongly or weakly subdominant. Under the generic assumption that the coefficients $\mathbf{b}_1$ and $\mathbf{b}_2$ of the initial data are linearly independent, we obtain with $\mathbf{n}_\infty := (\mathbf{b}_1 \times \mathbf{b}_2)/\|\mathbf{b}_1 \times \mathbf{b}_2\|$

$$\mathbf{n}_m = \mathbf{n}_\infty + \begin{cases} O\big(m^M \mu^m \lambda^{-m}\big) & \text{for an SSE} \\ O(1/m) & \text{for a WSE}\,. \end{cases}$$

Now, the second fundamental form is defined by

$$II_m = \begin{bmatrix} \langle \mathbf{n}_m, \partial_{uu} \mathbf{s}_m \rangle & \langle \mathbf{n}_m, \partial_{uv} \mathbf{s}_m \rangle \\ \langle \mathbf{n}_m, \partial_{uv} \mathbf{s}_m \rangle & \langle \mathbf{n}_m, \partial_{vv} \mathbf{s}_m \rangle \end{bmatrix}\,.$$

The computation of the inner products gives for instance

$$\begin{aligned}\langle \mathbf{n}_m, \partial_{uu}\mathbf{s}_m\rangle &= \left\langle \mathbf{n}_\infty + O(m^M\mu^m\lambda^{-m}), \lambda^m\partial_{uu}\boldsymbol{\varphi}(\mathbf{v}_1\mathbf{b}_1 + \mathbf{v}_2\mathbf{b}_1) + O(m^M\mu^m)\right\rangle \\ &= O(m^M\mu^m)\end{aligned}$$

for an SSE and

$$\begin{aligned}\langle \mathbf{n}_m, \partial_{uu}\mathbf{s}_m\rangle &= \left\langle \mathbf{n}_\infty + O(1/m), \tbinom{m}{L}\lambda^m\partial_{uu}\boldsymbol{\varphi}(\mathbf{v}_1\mathbf{b}_1 + \mathbf{v}_2\mathbf{b}_1) + O(m^{L-1}\lambda^m)\right\rangle \\ &= O(m^{L-1}\lambda^m)\end{aligned}$$

for a WSE. Since equivalent results hold for all other entries of the the second fundamental form, we obtain

$$I\!I_m = \begin{cases} O(m^M\mu^m) & \text{for an SSE} \\ O(m^{L-1}\lambda^m) & \text{for a WSE}\,. \end{cases} \tag{8}$$

3.5. Integrability Result

The principal curvatures κ_m^1, κ_m^2 are the negative eigenvalues of the differential of the Gauss map $dN_m = -I\!I_m I_m^{-1}$. Hence, their magnitude does not exceed that of dN_m, and Eqs. (7) and (8) imply the following asymptotic behavior.

Theorem 1. Consider a symmetric stationary linear subdivision scheme near an irregular vertex according to (1), (2). The subdivision matrix S has leading eigenvalues $1, \lambda, \lambda, \mu$ with algebraic multiplicities $1, L, L, M$, respectively, according to (6). Then, for almost all initial data $\mathbf{B}_0$, the principal curvatures $\kappa_m^{1,2}$ of the sequence of spline rings $\mathbf{s}_m, m \in \mathbb{N}$, satisfy

$$\kappa_m^{1,2} = O(I\!I_m I_m^{-1}) = \begin{cases} O(m^M\lambda^{-2m}\mu^m) & \text{for an SSE} \\ O(m^{-L-1}\lambda^{-m}) & \text{for a WSE}\,, \end{cases} \tag{9}$$

where the first case refers to a strongly subdominant eigenvalue, i.e., $L = 0$, and the second case refers to a weakly subdominant eigenvalue, i.e., $L > 0$.

Let us briefly discuss this result. In case of an SSE, the ratio $\rho := |\mu|/\lambda^2$ is crucial. If $\rho < 1$, then the principal curvatures tend to zero corresponding to an enforced flat spot at the irregular point. This case is studied in detail in [16]. If $\rho > 1$, then the principal curvatures diverge like ρ^m. If $\rho = 1$, then the principal curvatures are bounded if μ is simple ($M = 0$), or divergent at an algebraic rate otherwise ($M > 0$).

To obtain bounded curvatures rather than decay or divergence standard algorithms have been tuned to reveal this behavior [1,2,9,19]. However, the hitherto unknown influence of the multiplicity M of the eigenvalue μ has so far not been taken into account and should be checked for such schemes.

A measure for the regularity of curvatures is their integrability when raised to some power p, i.e., their membership in L_p-spaces. With the surface element

$$d\mathbf{s}_m = \|\partial_u \mathbf{s}_m \times \partial_v \mathbf{s}_m\| \, dudv = \sqrt{I_m} \, dudv = O\big(m^{2L}\lambda^{2m}\big) \, dudv$$

we obtain for the L_p-norm of the principal curvatures

$$\|\kappa_m^i\|_{p,m}^p := \int_{\mathbf{s}_m} |\kappa_m^i|^p \, d\mathbf{s}_m = \begin{cases} O\big(m^{pM}(\lambda^{-2p+2}\mu^p)^m\big) & \text{for an SSE} \\ O\big(m^{p(-L-1)+2L}(\lambda^{-p+2})^m\big) & \text{for a WSE}\,. \end{cases}$$

Using the fact that the series $\sum_{m=0}^{\infty} m^\alpha \beta^m$ converges if and only if $|\beta| < 1$ or $|\beta| = 1$ and $\alpha < -1$, we obtain the main result of this report.

Theorem 2. Consider a symmetric stationary linear subdivision scheme near an irregular vertex accoring to (1), (2). The subdivision matrix S has leading eigenvalues $1, \lambda, \lambda, \mu$ with algebraic multiplicities $1, L, L, M$, respectively, according to (6). For $p \geq 1$, denote the L_p-norm of the principal curvatures of the generated subdivision surface near the irregular point by

$$\|\kappa^{1,2}\|_p := \left(\sum_{m=0}^{\infty} \|\kappa_m^{1,2}\|_{p,m}^p \right)^{1/p}.$$

Then $\|\kappa^{1,2}\|_p$ is finite for almost all initial data $\mathbf{B}_0$ if

$$\begin{cases} p < \frac{2\ln|\lambda|}{2\ln|\lambda| - \ln|\mu|} & \text{for an SSE and} \quad \mu > \lambda^2 \\ p < \infty & \text{for an SSE and} \quad \mu = \lambda^2,\ M > 0 \\ p \leq \infty & \text{for an SSE and} \quad \mu = \lambda^2,\ M = 0 \quad \text{or} \quad \mu < \lambda^2 \\ p \leq 2 & \text{for a WSE}\,, \end{cases}$$

where SSE refers to a strongly subdominant eigenvalue, i.e., $L = 0$, and WSE refers to a weakly subdominant eigenvalue, i.e., $L > 0$.

Figure 6 illustrates the first case by showing the dependency of the limit exponent $p^* := 2\ln|\lambda|/(2\ln|\lambda| - \ln|\mu|)$ on μ for several values of λ. Since $\mu < \lambda$, it is clear that p^* is always greater than 2. This implies the following corollary, which is important for the application of subdivision surfaces to fourth order finite element problems.

Corollary 1. For almost all initial data, the principal curvatures of a subdivision scheme according to Theorem 2 are square integrable.

Following the ideas presented here, it can be shown that the latter statement is true for all generic C^1-subdivision schemes, as classified in [18] and [23].

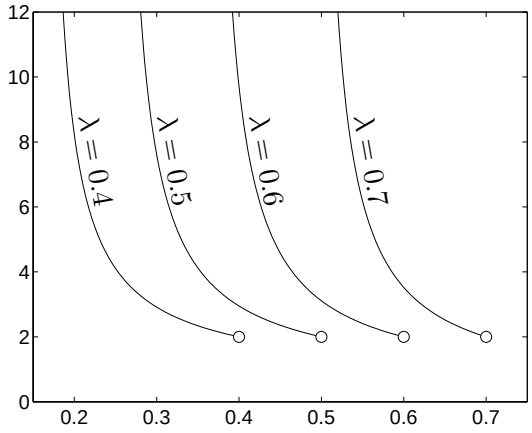

Figure 6. Limit exponent p^* in dependence on the third eigenvalue μ.

4. Examples

In this section we give some numerical examples of the curvature behavior near irregular points using Loop subdivision as a representative subdivision scheme. Additionally we briefly review the treatment of thin shell problems with the FEM, our original motivation for the analysis provided in this paper.

4.1. Numerical Curvature Computations

Figure 7 shows the result of computing curvatures numerically in the vicinity of a vertex of valence 8. Four different subdivision rules are compared. The classic rule with the weights proposed by Warren as well as three rules based on the spectrum manipulation described in Biermann et al. [2]. In the latter cases μ was set to values 0 (zero curvature), $(1-10^{-6})\lambda$ (formally admissable, but numerically approaching a case in which the surface is not even C^1), and λ^2 (bounded curvature). The bottom graph shows the result when the numerically computed values are renormalized with respect to our asymptotic estimates from Equation (9) showing perfect agreement (i.e., horizontal asymptotes). The actual surfaces corresponding to these settings are shown in Figure 8. Except for the extreme cases of zero curvature (flat spot; top right) and (almost) equal eigenvalues (pinch point; bottom right) the differences between a classic rule (top left) and a bounded curvature tuned rule (bottom left) are rather subtle. The classic rule reveals in its shading a slight hint of the pinch shown in the extreme in the bottom right, but is otherwise almost indistinguishable from the bounded curvature version.

It is well known from practical experience that vertices with very high valence are problematic in their appearance when modeling with subdivision surfaces. This visual loss of smoothness is also reflected in a decrease in smoothness when considering p as a function of valence for the classic weights as illustrated in Figure 9. While the surface has continuous curvatures for valence 6, the smoothness exponent p rapidly decreases as

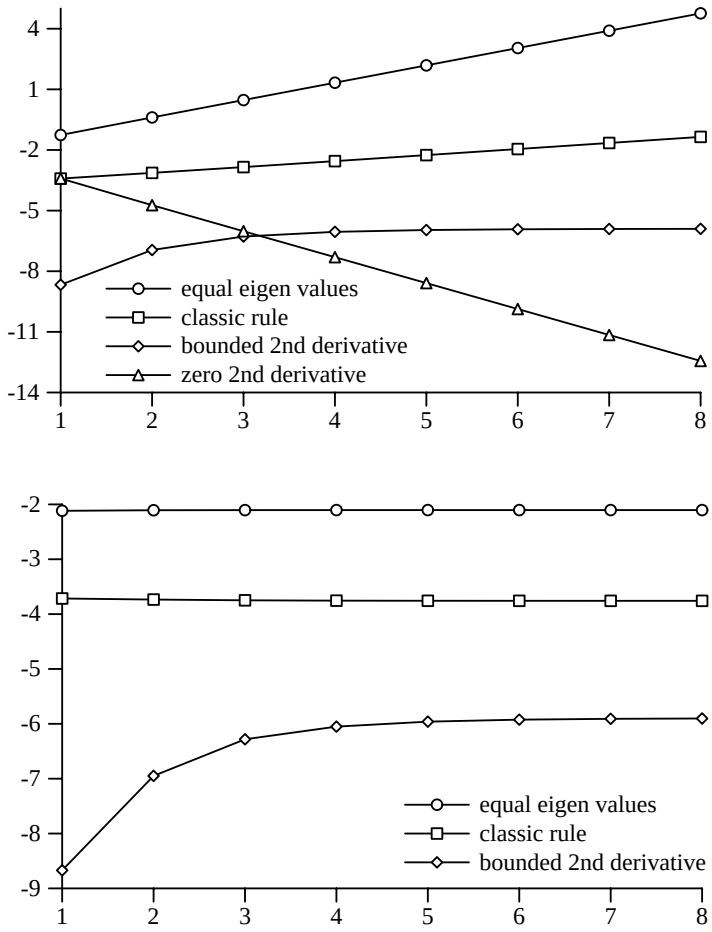

Figure 7. Comparison of numerically computed curvature for a valence 8 vertex with different eigenspectra. The top graph shows the logarithm of the actually computed values as a function of m, while the bottom graph shows the same data renormalized with respect to the asymptotically predicted values.

the valence increases. The limiting value being $p = 2$ as the valence goes to infinity (μ goes to λ from below).

4.2. FEM Treatment of Thin Shell Equations

Many areas of applied engineering design deal with thin flexible structures, for example those found in the automobile and aerospace industries. Their mechanical behavior can be described with Kirchhoff-Love theories [21] and is governed by the thin shell equations. These equations express the force balance between externally applied loads and internal forces due to stretching and bending. The latter are a function of the metric and curvature tensors of the surface. For example, the Green-Lagrange strain tensor is defined as the difference between the metric tensors of the deformed and undeformed

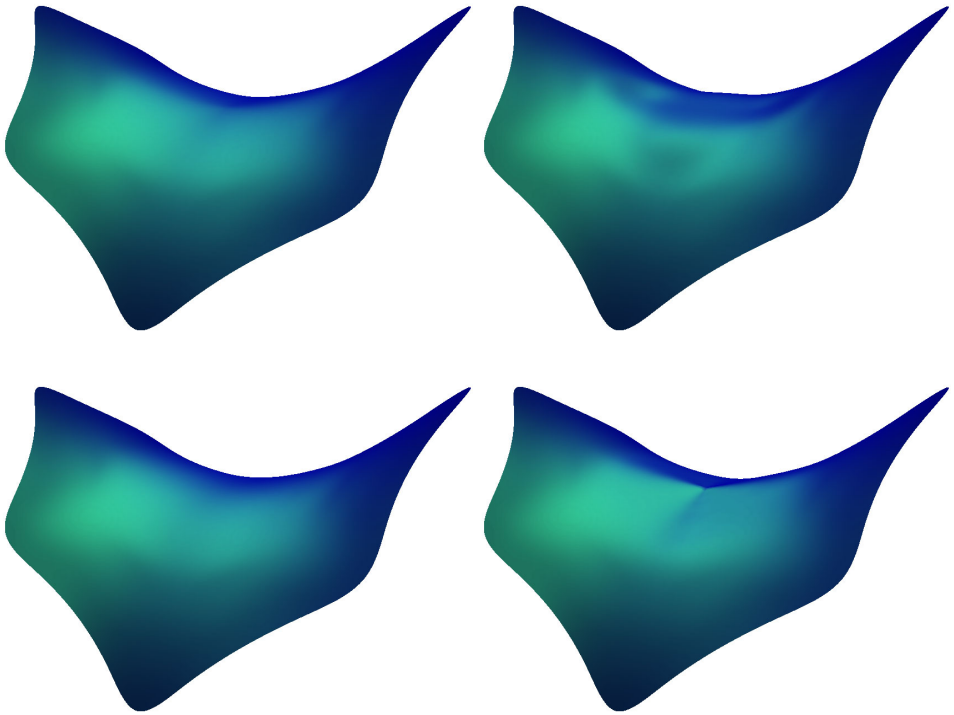

Figure 8. Renderings of a surface in the vicinity of a vertex of valence 8 for the different spectra considered in Figure 7: classic rule (top left), zero 2^{nd} derivative (top right), bounded curvature (bottom left), equal eigenvalues (bottom right). Note that the classic rule reveals a slight shadow of a pinch (a much milder version of the equal eigenvalue case) where the bounded curvature rule is noticeably smoother.

configuration respectively

$$E_{ij} = 1/2(g_{ij} - \bar{g}_{ij}), i, j = 1, 2.$$

Here $g_{ij} = g_i \cdot g_j$ are the covariant components of the metric tensor in the deformed configuration (the undeformed configuration variables carry an overbar). The thin shell is parameterized with respect to the middle surface and a normal displacement governing its thickness. Consequently E_{ij} contains terms arising from differences of the metric and curvature tensors of the surface (for more details see [4]). The resulting energy minimization problem is solved in the standard way through the calculus of variations. Linearizing the deformed configuration with respect to the undeformed configuration and applying the finite element discretization results in a linear system

$$K\Delta\mathbf{B}_0 = f$$

relating the unknown displacement degrees of freedom $\Delta\mathbf{B}_0$ between undeformed and deformed configurations to the externally applied forces f via the stiffness matrix K, whose entries are integrals involving as highest order terms products of curvatures of the

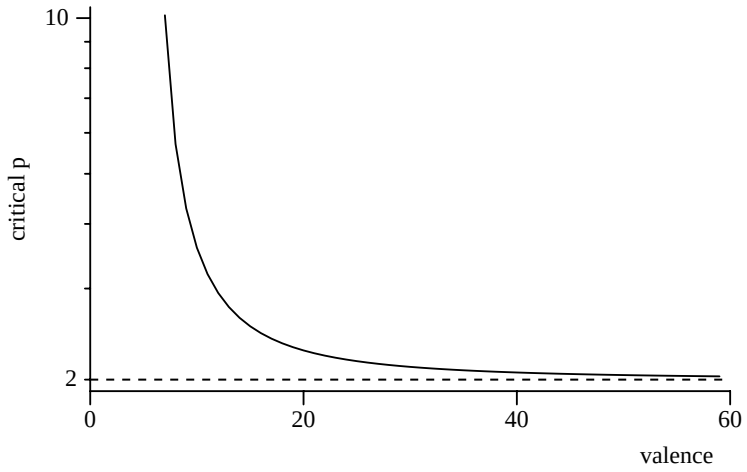

Figure 9. Smoothness p as a function of valence for the classic scheme. It quickly approaches the asymptotic value of $p = 2$ since $\mu \to \lambda$.

shape functions. Consequently the shape functions used in a FEM approach to thin shell equation modeling must have square integrable curvatures.

Figure 10 shows a simple example using these ideas. A cylinder is clamped at both ends while a point force is applied in the center pulling on the cylinder walls. The simulation takes the geometric non-linearities (dependence of K on $\mathbf{B}_0$) into account to model finite displacements.

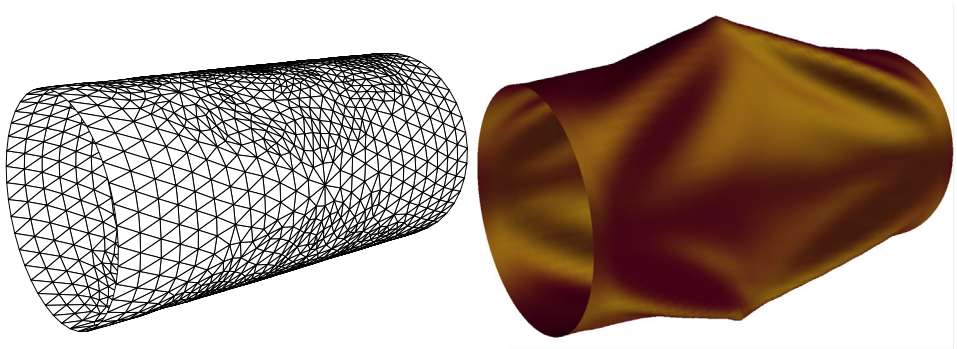

Figure 10. Thin shell simulation of a cylinder clamped at the ends using the scheme of Loop. A pair of point forces is pulling at the center while the ends are held by a rigid diaphragm. On the left the control mesh visualizing the actual degrees of freedom of the solver. On the right an image of the deformed limit surface. Simulation courtesy Fehmi Cirak, Caltech.

The properties of subdivision surfaces shown in this paper are a necessary ingredient in a unified representation of free form geometry and the simulation of its mechanical properties. This results in much simplified and considerably more robust codes. An ad-

ditional benefit is the excellent accuracy and convergence of FEM methods based on the use of subdivision shape functions [4].

Acknowledgements

The second author was supported in part by NSF (ACI-9624957, ACI-9721349, DMS-9874082, DMS-9872890), Alias|Wavefront and through a Packard Fellowship. Special thanks for Cici Koenig for production help and Fehmi Cirak and Eitan Grinspun for the thin shell simulation of the cylinder.

References

[1] BALL, A., AND STORRY, D. An investigation of curvature variations over recursively generated B-spline surfaces. Tech. rep., Loughborough University of Technology, 1990.

[2] BIERMANN, H., LEVIN, A., AND ZORIN, D. Piecewise Smooth Subdivision Surfaces with Normal Control. *Computer Graphics (Siggraph 2000 Proceedings)* (2000), 113–120.

[3] CATMULL, E., AND CLARK, J. Recursively Generated B-Spline Surfaces on Arbitrary Topological Meshes. *Computer Aided Design 10*, 6 (1978), 350–355.

[4] CIRAK, F., ORTIZ, M., AND SCHRÖDER, P. Subdivision Surfaces: A New Paradigm for Thin-Shell Finite-Element Analysis. *Int. J. Numer. Meth. Engng. 47* (2000).

[5] COHEN, E., LYCHE, T., AND RIESENFELD, R. Discrete B-splines and Subdivision Techniques in Computer Aided Geometric Design and Computer Graphics. *Computer Graphics and Image Processing 14*, 2 (1980), 87–111.

[6] DOO, D., AND SABIN, M. Analysis of the Behaviour of Recursive Division Surfaces near Extraordinary Points. *Computer Aided Design 10*, 6 (1978), 356–360.

[7] DYN, N., LEVIN, D., AND GREGORY, J. A. A Butterfly Subdivision Scheme for Surface Interpolation with Tension Control. *ACM Trans. Gr. 9*, 2 (April 1990), 160–169.

[8] HABIB, A., AND WARREN, J. Edge and Vertex Insertion for a Class of C^1 Subdivision Surfaces. *CAGD 16*, 4 (1999), 223–247. Previously available as a TR, Rice University, August 1997.

[9] HOLT, F. Towards a curvature-continuous stationary subdivision algorithm. *Z. Angew. Math. Mech. 76* (1996), 423–424. Suppl. 1.

[10] HOPPE, H., DEROSE, T., DUCHAMP, T., HALSTEAD, M., JIN, H., MCDONALD, J., SCHWEITZER, J., AND STUETZLE, W. Piecewise Smooth Surface Reconstruction. In *Computer Graphics Proceedings*, Annual Conference Series, 295–302, 1994.

[11] KOBBELT, L. Interpolatory Subdivision on Open Quadrilateral Nets with Arbitrary Topology. In *Proceedings of Eurographics 96*, Computer Graphics Forum, 409–420, 1996.

[12] LEBER, M. Interpolierende Unterteilungsalgorithmen. Master's thesis, Universität Stuttgart, 1994.

[13] LOOP, C. Smooth Subdivision Surfaces Based on Triangles. Master's thesis, University of Utah, Department of Mathematics, 1987.

[14] PETERS, J., AND REIF, U. The Simplest Subdivision Scheme for Smoothing Polyhedra. *ACM Transactions on Graphics 16*, 4 (October 1997), 420–431.

[15] PETERS, J., AND REIF, U. Analysis of Algorithms Generalizing B-Spline Subdivision. *SIAM Jornal of Numerical Analysis 35*, 2 (1998), 728–748.

[16] PRAUTZSCH, H., AND UMLAUF, G. G^2-continuous subdivision algorithm. Preprint, 1997.

[17] REIF, U. A Unified Approach to Subdivision Algorithms Near Extraordinary Points. *Comput. Aided Geom. Des. 12* (1995), 153–174.

[18] REIF, U. *Analyse und Konstruktion von Subdivisionsalgorithmen für Freiformflächen beliebiger Topologie*. Shaker Verlag, 1999. Habilitationsschrift.

[19] SABIN, M. A. Cubic Recursive Subdivision with Bounded Curvature. In *Curves and Surfaces*, Laurent, L. Mehaute, and Schumaker, Eds. 1991, pp. 411–414.

[20] SCHWEITZER, J. E. *Analysis and Application of Subdivision Surfaces*. PhD thesis, University of Washington, 1996.

[21] TIMOSHENKO, S., AND WOINOWSKY-KRIEGER, S. *Theory of Plates and Shells*. McGraw-Hill Book Company Inc., 1959.

[22] WARREN, J. Subdivision Methods for Geometric Design. Unpublished manuscript, November 1995.

[23] ZORIN, D. Smoothness of subdivision on irregular meshes. *Constructive Approximation 16*, 3 (2000), 359–397.

[24] ZORIN, D., AND SCHRÖDER, P., Eds. *Subdivision for Modeling and Animation*. Course Notes. ACM SIGGRAPH, 1999.

[25] ZORIN, D., SCHRÖDER, P., AND SWELDENS, W. Interpolating Subdivision for Meshes with Arbitrary Topology. *Computer Graphics (SIGGRAPH '96 Proceedings)* (1996), 189–192.